

# A $4\pi$ BaF<sub>2</sub> detector for (n, $\gamma$ ) cross section measurements at a spallation neutron source

M. Heil<sup>a</sup>, R. Reifarh<sup>a</sup>, M.M. Fowler<sup>b</sup>, R.C. Haight<sup>b</sup>,  
F. Käppeler<sup>a</sup>, R.S. Rundberg<sup>b</sup>, E.H. Seabury<sup>b</sup>, J.L. Ullmann<sup>b</sup>,  
J.B. Wilhelmy<sup>b</sup>, K. Wisshak<sup>a</sup>

<sup>a</sup>*Forschungszentrum Karlsruhe, Institut für Kernphysik, P.O. Box 3640, D-76021  
Karlsruhe, Germany*

<sup>b</sup>*Los Alamos National Laboratory, Los Alamos, NM 87545, USA*

---

## Abstract

The quest for improved neutron capture cross sections for advanced reactor concepts, transmutation of radioactive wastes as well as for astrophysical scenarios of neutron capture nucleosynthesis has motivated new experimental efforts based on modern techniques. Recent measurements in the keV region have shown that a  $4\pi$  BaF<sub>2</sub> detector represents an accurate and versatile instrument for such studies. The present work deals with the potential of such a  $4\pi$  BaF<sub>2</sub> detector in combination with spallation neutron sources, which offer large neutron fluxes over a wide energy range. Detailed Monte Carlo simulations with the GEANT package have been performed to investigate the critical backgrounds at a spallation facility, to optimize the detector design, and to discuss alternative solutions.

---

## 1 Introduction

The development of intense spallation neutron sources [1, 2] has made possible the measurement of neutron capture cross sections on submilligram samples [3, 4]. This is a necessary development for neutron cross section measurements of rare isotopes, especially radioactive isotopes. The new capabilities of these neutron sources are applicable to basic research on the nature of the neutron capture process, applied research in support of the accelerator transmutation of radioactive waste (ATW), research in support of nuclear astrophysics research, as well as other applications. The neutron energy range over which cross sections need to be measured for our specific applications is below 1 MeV, where the capture cross sections are generally large, where the ATW

schemes often have large neutron fluxes, and where astrophysical nucleosynthesis takes place for producing s-process isotopes and in the later stages of the r and p processes.

These applications make certain demands on the overall performance of the neutron time-of-flight spectrometer, including the  $\gamma$ -ray detector array. The spectrometer must be able to make accurate measurements of neutron capture on small targets, e.g. submilligram, because the isotopes are inherently difficult to produce and in some cases have a very high specific radioactivity. High detector efficiency is desired for good counting statistics, for minimizing corrections for missed events, and for measuring the total energy emitted as  $\gamma$ -rays. With good energy resolution and a well defined efficiency response function, true capture events can be distinguished from the random  $\gamma$ -rays emitted from radioactive targets and from many sources of background capture events simply by demanding that the detected total energy of the gamma rays be equal to the Q-value of the desired capture reaction plus the kinetic energy of the incident neutron.

Of particular importance also is the sensitivity of the detector to neutrons, both those scattered from the target and target backing as well as background from other sources. With pulsed monoenergetic sources, the background from neutrons scattered by the sample can often be separated cleanly from the capture  $\gamma$ -ray events by time-of-flight (TOF) techniques. Even if the detector captures the scattered neutrons, these events come much later than  $\gamma$ -rays from neutron capture on the sample. For example, the flight time of a 100 keV neutron over a 10 cm path is 22.9 ns, entirely adequate for distinguishing it from a capture  $\gamma$ -ray. Unfortunately, this technique cannot be applied to neutron TOF spectrometers with so-called “white” neutron sources because of the wide range in neutron energy (subthermal to several hundred MeV). With a white neutron source, scattered neutrons can arrive at the detector at the same time as capture  $\gamma$ -rays from slower neutrons. A very instructive example of this has been given by Guber et al. [5]. The design must therefore compensate for this shortcoming in order to make measurements of the accuracy previously achieved with monoenergetic or nearly monoenergetic sources [6].

Despite this disadvantage of white neutron sources, they have very strong advantages. Resonance properties can be studied thoroughly as the neutron energy sweeps through the resonances; the energy range is continuous from subthermal to well over 1 MeV; and techniques are well developed for measurements of neutron flux and various sources of backgrounds.

White neutron sources are based on electron linear accelerators or medium or high energy proton accelerators, which produce neutrons by spallation reactions. Although a proper comparison depends on many parameters, spallation

sources typically have intensities greater than those of electron linacs by several orders of magnitude in the region below a few tens of keV. A comparison of the LANSCE spallation neutron source with those based on electron linacs has been given previously [7]. A further advantage is that the “gamma flash” of electron linacs is significantly reduced in spallation sources, although the latter do produce a large flux of high energy (up to several hundred MeV) neutrons. Although present spallation sources, designed mostly for condensed matter research, have a worse time spread than electron linac sources, this is not an inherent limitation, and future sources [2] could be designed to reduce this difference. Because of the advantages of spallation neutron sources, we focus our discussion on them, although many characteristics of the detectors in our design would be useful also at other white neutron sources.

To effectively use the new capabilities of spallation neutron sources, new techniques and new detectors will be required. In this paper, we discuss the potential for a highly segmented array of BaF<sub>2</sub> detectors surrounding the sample in which the capture cross section is to be measured. This detector array is segmented so that it can handle the radiations from the radioactive decay which might have the intensity of a Curie ( $3.7 \times 10^{10}$  Bq) or more. We prefer an array that acts as a calorimeter in the sense that the total  $\gamma$ -ray energy from a capture event is measured; this approach is very useful in separating capture events on the sample from those on other materials in the region.

In this paper we first discuss the general requirements for a  $4\pi$  detector. We then compare the results of a GEANT simulation to the measured parameters of the Karlsruhe 42-detector array to validate the calculational approach. Finally, we apply GEANT to simulate a proposed 162-element BaF<sub>2</sub> array for use at the LANSCE spallation neutron source, and a similar array proposed for use at CERN.

Other  $4\pi$  arrays of scintillators have been developed, e.g. for research in light and heavy ion reactions [8]. Originally, these detector arrays have relied on NaI(Tl) or CsI(Tl or pure) as the scintillation materials. Our designs are based to a large extent on the geometries of those arrays. In neutron capture reaction studies, an array of 8 elements of BaF<sub>2</sub> was developed previously for use at LANSCE [9], and BaF<sub>2</sub> has been used also in single or small arrays with lower efficiency [5]. The  $4\pi$  array of 42 detectors at Karlsruhe [10, 11, 12] in use with a low energy neutron source has proved to be extremely productive in the field of cross section measurements for nuclear astrophysics, and we base much of our design considerations on that instrument.

With the simulations reported here, we believe that greater confidence can be had in the choice of design of the new detector systems.

## 2 Requirements of a $4\pi$ detector

### 2.1 *General aspects*

The principle of using a  $4\pi$  detector with high  $\gamma$ -ray efficiency and reasonably good resolution is a complete detection of the prompt  $\gamma$ -ray cascade emitted in a capture reaction. This concept offers the advantage of obtaining a clear signature for capture events via the sum energy of  $\gamma$  cascades, which reflects the binding energy of the captured particle. Provided that the detector is segmented into a sufficiently large number of independent modules, valuable additional information on event multiplicities and hit patterns can be obtained as well. Accordingly true capture events can be reliably distinguished from  $\gamma$ -backgrounds which are inherent to neutron experiments.

In this respect  $4\pi$  arrays differ completely from the simpler approach based on the detection of single capture  $\gamma$ -rays. This category uses detectors with  $\gamma$ -ray efficiencies which are linearly increasing with  $\gamma$ -energy. It includes Moxon-Rae type detectors [13, 14], where this feature is approximated by a  $\gamma$ -ray converter followed by a thin plastic scintillator, as well as the commonly used and confusingly named “total energy” detectors. The latter design is based on  $C_6D_6$  or  $C_6F_6$  liquid scintillators of typical 1 l volume, which allow the detection of capture events with  $\approx 20\%$  efficiency but require an external weighting function for obtaining the linear relationship between  $\gamma$ -ray energy and efficiency [15]. These detectors, which are currently in use at electron linear accelerators [16, 17], do not provide sufficient gamma-ray energy information to differentiate capture on the sample from capture of scattered neutrons on nearby materials. Hence, corrections for the various backgrounds discussed below are much more difficult to determine.

### 2.2 *Choice of Scintillator*

The main problem in using  $4\pi$  arrays results from their much larger detector volume and from the fact that the chemical composition of the inorganic scintillator may include isotopes with relatively large cross sections for neutron capture. This makes them much more sensitive to neutrons scattered by the sample. Particularly for keV neutron energies, where scattering in the sample dominates over capture, subsequent capture of the scattered neutrons in the scintillator can increase the overall systematic uncertainty. These effects reduce the number of suitable scintillator materials. For example, NaI and CsI have to be excluded from this application because of the large iodine ( $n,\gamma$ ) cross section. Several suitable scintillators are listed in Table 1, all being composed

Table 1

Characteristics of some scintillator materials

Scintillator	Density (g/cm <sup>3</sup> )	Decay time (ns)	Wavelength (nm)	Photons per MeV
BaF <sub>2</sub>	4.88	0.6; 630	220; 310	1800; 10000
Bi <sub>4</sub> Ge <sub>3</sub> O <sub>12</sub> (BGO)	7.13	60; 300	480	700; 7500
CeF <sub>3</sub>	6.16	3; 27	300; 340	200; 4300
C <sub>6</sub> F <sub>6</sub>	1.61	3.3	430	≈10000

Table 2

Neutron sensitivity of suited scintillators in different energy regions assuming a bare gold sample in a well collimated beam and neglecting the delay between capture of neutrons in the sample and capture of scattered neutrons in the scintillator.

Scintillator	Thickness (cm)	Capture of scattered neutrons/true captures in sample			
		0.1 to 1 keV	1 to 10 keV	10 to 100 keV	0.1 to 1 MeV
BaF <sub>2</sub>	15	0.52±0.02	1.09±0.04	1.34±0.10	3.19±0.60
Bi <sub>4</sub> Ge <sub>3</sub> O <sub>12</sub> (BGO)	10	0.35±0.02	0.84±0.05	1.24±0.14	2.22±0.61
CeF <sub>3</sub>	13	0.038±0.004	0.12±0.01	0.75±0.10	1.89±0.48
C <sub>6</sub> F <sub>6</sub>	60	0.035±0.004	0.018±0.005	0.036±0.014	1.28±0.37

of low cross section materials.

The choice of BaF<sub>2</sub> for the Karlsruhe 4 $\pi$  array [12] was based on the fact that it exhibits similar sensitivity to scattered neutrons compared to CeF<sub>3</sub> and bismuth germanate (BGO) but has the advantage of better time and energy resolution. The responses of the scintillators listed in Table 1 to scattered neutrons are compared in Table 2. (See Section V.C.8 for details of the calculation.) Here we assume scintillator volumes of equal  $\gamma$ -efficiency, a capture sample of gold, and a well collimated neutron beam. One finds that the organic C<sub>6</sub>F<sub>6</sub> scintillator has by far the smallest sensitivity for scattered neutrons, despite the large thickness required to match the efficiency of the high-Z materials in the inorganic scintillators. With BaF<sub>2</sub>, comparable values could only be reached using isotopically pure <sup>138</sup>Ba due to the very small (n, $\gamma$ ) cross section of this neutron magic nucleus.

To minimize the neutron sensitivity, all considered scintillators are composed of materials with small capture cross sections and hence large scattering/capture ratios. Accordingly, most scattered neutrons diffuse out of the 4 $\pi$  array without being captured. Typical diffusion times being of the order of 3  $\mu$ s imply that the related captures would appear as prompt background in experiments using long neutron flight paths, whereas most of the capture can be discriminated via time-of-flight in experiments carried out with very short flight paths

such as those used with low energy, monoenergetic sources.

### 2.3 Detector details

There are various possibilities to cover the full solid angle with an arrangement of closely packed crystals. In order to facilitate the interpretation of event multiplicities, the crystals should be shaped such that they cover equal solid angles. Such geometries are known to correspond to fullerene-type structures consisting of a few configurations with certain, fixed number of elements [8]. In this work two geometries with 42 and 162 crystals respectively were simulated.

The 42-element geometry using 30 hexagonal and 12 pentagonal crystals was adopted for the Karlsruhe  $4\pi$  BaF<sub>2</sub> detector [12]. In this approach, the crystals form a closed sphere with an inner diameter of 20 cm and a thickness of 15 cm, which is sufficient to detect gamma rays of a few MeV energy, the minimum of the absorption coefficient, with  $\geq 90\%$  efficiency. The geometry of this setup was modeled in detail, including the light reflector (Teflon) and the aluminum cladding of the individual detector modules. These simulations could be verified by comparison with the experimental performance of the detector (Sec. III).

The setup with 162 elements and therefore higher granularity is favored for experiments where high count rates or higher multiplicities are expected. This more complex geometry requires four different crystal shapes to cover the sphere uniformly, as shown in Fig. 1. A full model was also constructed for this geometry including all details used in the 42-fold scintillator array.

In order to find an optimized solution with respect to several design parameters, simulations were carried out for different crystal thicknesses and for different inner diameters of the  $4\pi$  detector. With a shell thickness of 15 cm a total efficiency of  $\geq 90\%$  for  $\gamma$ -rays in the relevant energy range could be achieved. Increasing the thickness of the crystals yields a higher efficiency but the larger detector volume implies more severe background due to capture of sample-scattered neutrons. For this reason and for controlling the overall costs, the inner diameter of the detector should be kept as small as possible though it was found that this background can be substantially reduced by means of a <sup>6</sup>LiH liner inside the detector sphere. In summary, an inner diameter of 20 cm and a crystal thickness of 15 cm was found to be a good compromise between detector performance and costs.

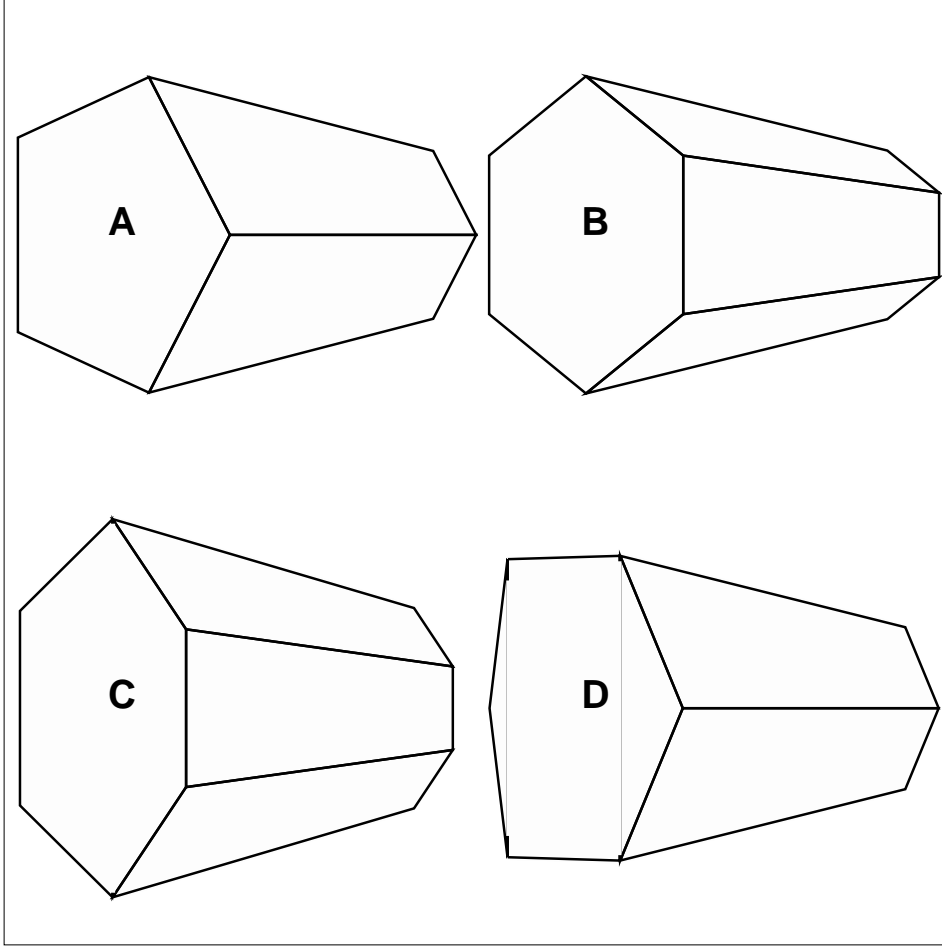


Fig. 1. A  $4\pi$  array with 42 modules can be built from 12 pentagons and 30 regular hexagons (see Ref. [12]). The 162-module design is also based on 12 regular pentagons of type A (left, top) but requires three different shapes for the hexagons, 30 regular crystals of type B, 60 of type C, and 60 of type D (right, bottom).

### 3 GEANT simulations

The performance of the various design options was simulated with the GEANT detector description and simulation tool from CERN [18]. GEANT tracks photons, electrons and hadrons, which in this case are only neutrons and protons. In this work, the GHEISHA module was used for tracking neutrons with energies above 200 keV, while the GCALOR [19] interface with the MICAP package was preferred for neutron energies below 200 keV. A 10 keV cut-off energy was chosen for all particles except for neutrons, where this limit was defined at 10 meV. Particles falling below these thresholds are assumed to deposit their residual kinetic energy without further interaction. In general, GCALOR considers pointwise cross section data from the ENDF/B-VI evaluation [20]. Additionally, theoretical  $\gamma$ -cascades for neutron capture events had

to be used for the barium isotopes and for gold [21, 22] since these photon data for neutron capture events were not available from this library.

The calculations account only for the energy deposited in the scintillators and neglect photon losses and the limited photo-efficiency of the photomultiplier tubes (PMTs). In the simulation these effects were considered by folding the calculated response with the experimentally determined energy resolution of the Karlsruhe  $4\pi$  BaF<sub>2</sub> detector, which uses both the short and long decay-time components of the light output, which together give about 11,800 photons per MeV. The effects of photon yields of the other scintillators and for using just one component of the BaF<sub>2</sub> scintillation light is to change the resolution approximately by the photon statistics,  $\approx 1/\sqrt{N}$ . For C<sub>6</sub>F<sub>6</sub> detectors, where the size of the scintillator must be very large in order to absorb the entire  $\gamma$ -ray energy, further losses of light are expected to reduce the resolution.

Since GEANT is a simulation tool developed for tracking high energy particles, the treatment of low-energy interactions may be uncertain by 20% [18]. This problem was checked by comparing GEANT simulations for monoenergetic  $\gamma$ -rays with the experimental spectra measured with the Karlsruhe array. In this experiment, the proton beam of the Van de Graaff accelerator was directed onto thin <sup>26</sup>Mg, <sup>30</sup>Si, and <sup>34</sup>S targets in the center of the detector. These targets exhibit (p, $\gamma$ ) resonances, which are known to produce pure two-step cascades. By replacing the BaF<sub>2</sub> crystal at zero degrees by a HPGe detector and by gating the response of the  $4\pi$  detector by requiring a full-energy signal in the Ge detector, the response of the Karlsruhe array to monoenergetic  $\gamma$ -rays could be measured for 22 energies from 0.843 MeV to 8.392 MeV [23]. The experimental spectra for 2.209 MeV and 6.146 MeV  $\gamma$ -rays are compared in Fig. 2 to the corresponding GEANT simulations. Obviously, the measured spectra are reproduced very well in the simulations, except for small deviations at lower energies due to the effect of differences in the electronic thresholds.

## 4 The Karlsruhe 42-Detector $4\pi$ Array

### 4.1 *The facility*

The Karlsruhe  $4\pi$  array is used for the determination of (n, $\gamma$ ) cross sections in the astrophysically relevant neutron energy range from 3 to 220 keV. The present simulation of this detector concentrated on the measured signature from the prompt capture  $\gamma$ -ray cascades and on the background due to sample-scattered neutrons which may be captured in materials of the scintillator (BaF<sub>2</sub>, Al, Teflon, etc.). With the Karlsruhe neutron source, time-of-flight information can be used to separate these two processes. The most impor-



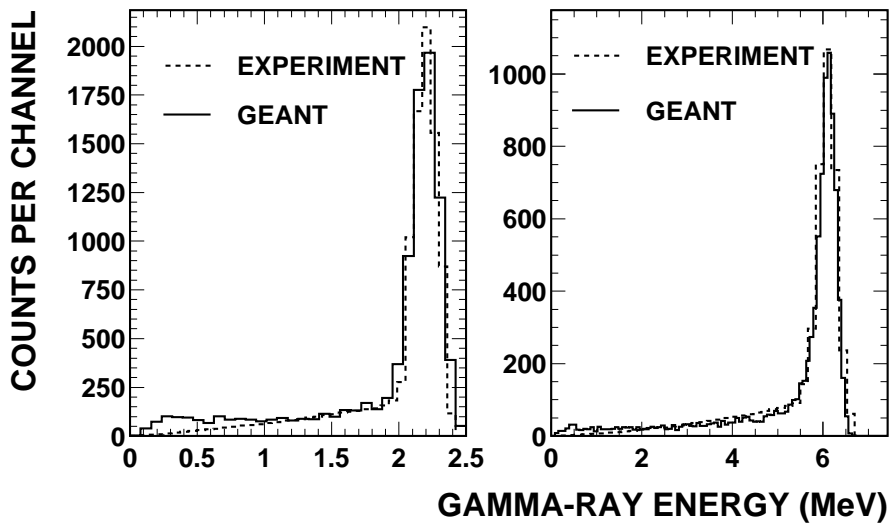


Fig. 2. Measured and simulated response of the Karlsruhe array of 42 BaF<sub>2</sub> modules to monoenergetic  $\gamma$ -rays.

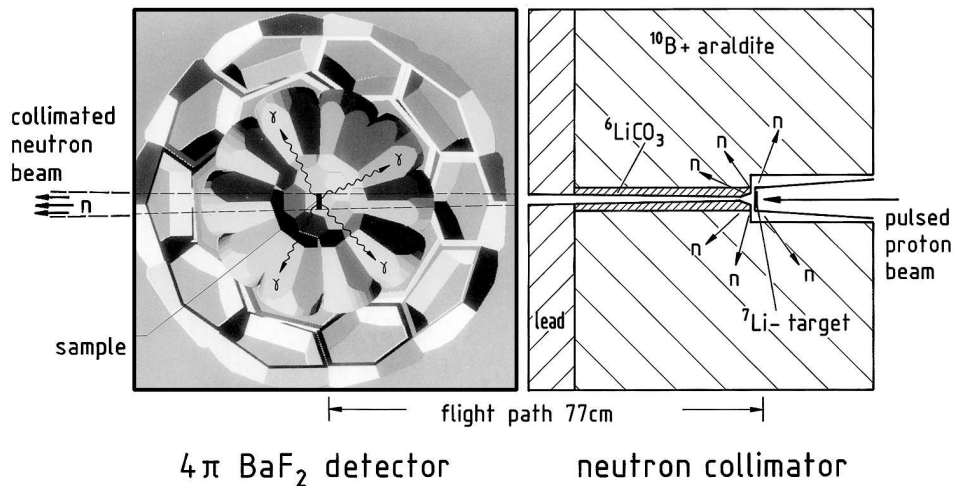


Fig. 3. The Karlsruhe setup for  $(n,\gamma)$  studies with the 42-module BaF<sub>2</sub> array.

tant features for characterizing these two components are the respective sum energy signals and the corresponding multiplicity distributions. Because the Karlsruhe detector is so well characterized, its performance can serve as a test and validation of the GEANT simulations.

The essential features of the experimental setup are sketched in Fig. 3. Neutrons with a continuous energy distribution are produced via the  ${}^7\text{Li}(p,n){}^7\text{Be}$  reaction by bombarding thin metallic lithium targets with the pulsed proton beam from a Van de Graaff accelerator (repetition rate 250 kHz, beam energy 1.9 to 2 MeV, average beam current  $2\ \mu\text{A}$ ). The collimated neutron beam hits the sample in the center of the detector array after a flight path of  $\approx 80$  cm.

## 4.2 *Response to gamma rays from capture on the sample*

The simulations required information on the original capture cascades, which were obtained either from the ENDF/B library that is part of the GCALOR software or from detailed theoretical calculations. Throughout this paper, the simulations refer to metallic gold samples. Since such samples are routinely used for neutron flux determination in all measurements with the  $4\pi$  detector, there are ample data available for comparison. In simulating the background from scattered neutrons (Section III.C), capture events in the various barium isotopes as well as in fluorine and reflector materials were considered.

The first example is presented in Fig. 4, showing the comparison between the experimentally measured sum-energy spectra of neutron captures in the gold sample [24] and the corresponding simulation. The spectra show two components: capture cascades which are completely detected and appear as a line at the binding energy of the captured neutron, and events where part of the energy of the cascade  $\gamma$ -rays escapes detection resulting in a tail towards lower energies. Both components are reproduced very well by the simulation.

It is quite remarkable that the successful agreement between experiment and simulation holds not only for the average of all events but rather well also for the different detector-hit multiplicities. The various multiplicity cuts contain only one normalization constant, the total number of events. In achieving this result it was also important to consider the internal conversion of low-energy  $\gamma$ -transitions in the theoretical cascades. Particularly for the gold sample, this effect caused a significant broadening of the peak toward lower total detected energy.

## 4.3 *Response to scattered neutrons*

In a further step, the background from sample-scattered neutrons was simulated for the experimental TOF spectra. The left part of Fig. 5 shows a typical experimental TOF spectrum, the edge at short times reflecting the maximum neutron energy of 130 keV. The cut-off at  $1.15 \mu\text{s}$  corresponds to the software window for suppressing the neutron energy range below 2.5 keV, which is dominated by the background from scattered neutrons. The same data are plotted in the right part of Fig. 5 but projected on the  $\gamma$ -energy axis, illustrating the advantage of a calorimetric measurement with good energy resolution. This spectrum exhibits a number of peaks corresponding to capture events in different isotopes in the detector, thus allowing unambiguous background assignments.

Again, both spectrum types in Fig. 5 are fitted very well by the simulations.

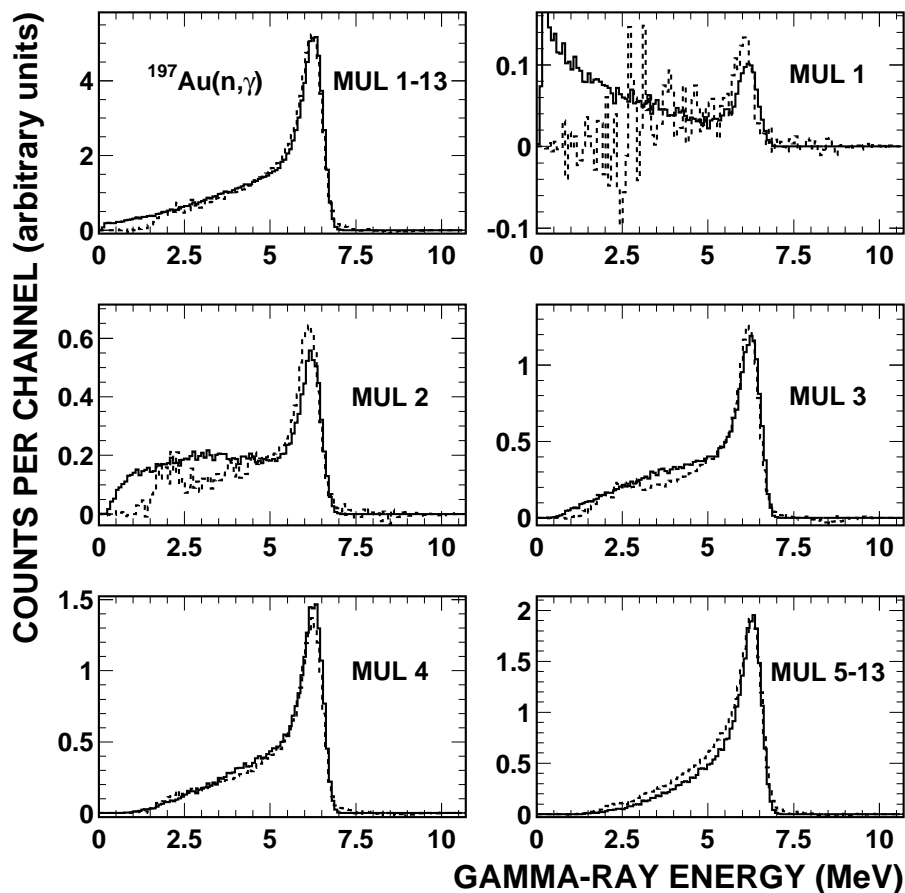


Fig. 4. Measured (dashed curve) and simulated (solid curve) response of the Karlsruhe  $4\pi$  detector to neutron captures in  $^{197}\text{Au}$ . The spectrum averaged over all events is shown in the left panel in the top row. The spectra for events with different multiplicities can also be well reproduced.

The quality of the simulations can be appreciated by the significance of the small differences in the right spectrum, which were identified as being due to errors in the original barium cross sections used in the ENDF/B-VI library. Recently, this discrepancy could be explained on the basis of improved Ba cross section data [25].

In summary, these examples studied in this section indicate that the rather complex geometry of a  $4\pi$  detector of high granularity can be successfully described. The successful simulation of the detector response to monoenergetic  $\gamma$ -rays as well as to the experimental situation of an actual measurement makes the GEANT software a reliable tool for studying and optimizing this type of detectors in a variety of applications.

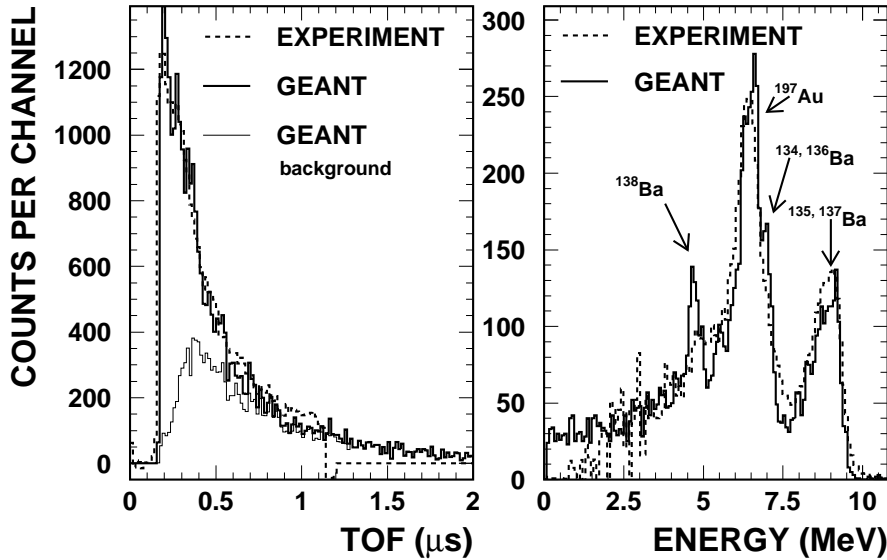


Fig. 5. Simulation of background due to capture of scattered neutrons in the Karlsruhe array. Left: Comparison for a TOF spectrum. Right: The  $\gamma$ -ray spectrum of the same events showing that different background reactions in the even and odd Ba isotopes can be distinguished.

## 5 GEANT simulations for setup at spallation sources

### 5.1 General Considerations

Neutron capture experiments at a spallation, white neutron source face challenges not encountered at monoenergetic or quasi-monoenergetic sources. Firstly, because of the long flight path between the source and sample and because of the presence of higher energy neutrons, time-of-flight cannot be used to differentiate neutrons captured in the sample from neutrons scattered by the sample and subsequently captured in the  $\text{BaF}_2$  scintillator. Moderation and absorption of the scattered neutrons is an approach to reduce this background. Secondly, collimation of the higher energy neutrons is more difficult and the ambient background is likely to be higher. Because these effects are specific to individual flight paths at given facilities, only the effect of an assumed beam halo is discussed here. Thirdly, the duty factor of monoenergetic sources is high, sometimes nearly 100%. Spallation sources typically have repetition rates of 20 to 30 Hz [7] and the new source at CERN is planned to run between 0.4 and 0.07 Hz [2]. Longer running times are therefore needed at spallation neutron sources if the number of events per beam burst is the same. However, the instantaneous rate at spallation sources is much higher, which enables the use of small samples of very radioactive materials. The high instantaneous rate, however, requires that new techniques be developed to handle the large

amounts of data.

Unless otherwise specified, all following simulations refer to a 160 crystal  $\text{BaF}_2$  array (162 elements with vacant entrance and exit positions to accommodate the beam tube), a  $1/E$  approximation to the neutron spectrum expected for the LANSCE TOF facility at 20 m flight path [27], and a gold sample in the center of the array. Note that gold is a relatively forgiving sample as far as the scattering background is concerned, the scattering/capture ratio ranging between 10 and 100 at keV neutron energies. For other possible samples, the ratio can range to well over 1000 and the discrimination against capture of scattered neutrons by the detector material is then more challenging.

## 5.2 Spallation Neutron Spectra

The neutron spectra from spallation neutron sources have been discussed previously [7, 26]. For the present considerations, the neutron spectrum is that emitted from a moderator near the primary neutron production site to enhance the neutron flux below 100 keV. At LANSCE this spectrum has been measured to be  $E^{-0.948}$ , which is very close to  $1/E$ , up to 100 keV [9, 27]. The shape of the spectrum at higher energies has been calculated and needs to be measured. For the LANSCE simulations reported here, we assume that the spectrum continues as  $1/E$  at all energies. The CERN facility is still in the planning stages and for its neutron spectrum we rely on calculations [2]. Note that there is an increase over the  $1/E$  shape at neutron energies between 10 keV and 1 MeV.

## 5.3 Response to scattered neutrons

### 5.3.1 Baseline calculation

As in the Karlsruhe setup, the capture detector at a spallation neutron source will be sensitive to neutrons scattered from the sample. With the 20 meter flight path and the  $1/E$  neutron spectrum at LANSCE, pulse height spectra were calculated for flight times corresponding to neutrons in the range 0.1 to 1eV, 1 eV to 10 eV, and so forth. Pulses due to true capture events on the gold sample were tallied and compared with pulses due to scattered neutrons captured in the detector. The results, given in Fig. 6, show that the neutron sensitivity of the detector becomes important for times corresponding to neutron energies above 1 keV. Above 100 keV, the detector response is dominated by events due to these scattered neutrons.

In the following subsections, we discuss design parameters that affect the abil-

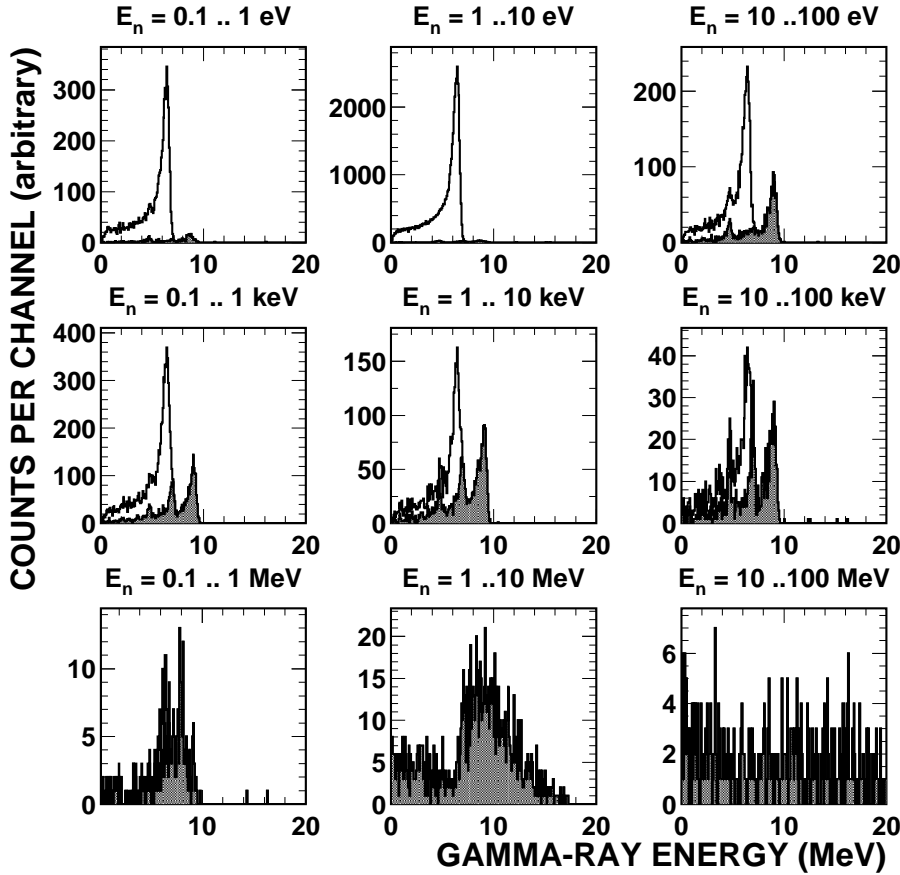


Fig. 6. Simulated  $\gamma$ -ray spectra (solid line) for capture events expected at the neutron spectrum of a spallation source. The respective background due to scattered neutrons (shaded area) is indicated for different time-of-flight bins.

ity to differentiate true capture events from those due to scattered neutrons.

### 5.3.2 Flight path lengths

Apart from the good resolution in time-of-flight, the 200 m flight path proposed at CERN [2] eases also the task of discriminating between true capture events and those related to capture of neutrons scattered from the sample. The reason is that at CERN there will be more separation in time between neutrons of different energies. The scattering of higher energy neutrons from the sample (where the scattering-to-capture ratio is very high) will thus be more easily separated from the desired capture events from lower energy neutrons, an effect which can be important in case of resonance-dominated cross sections.

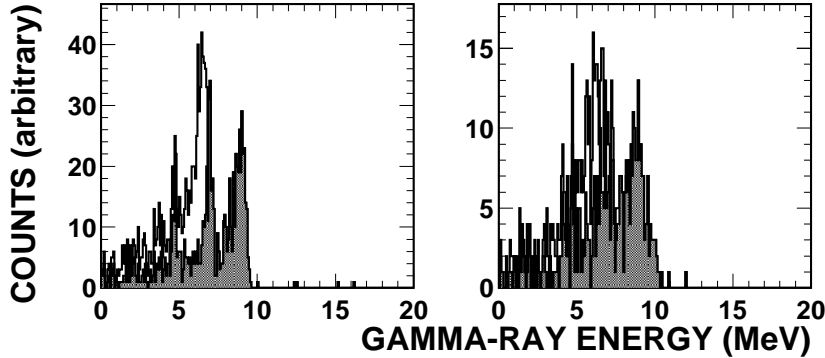


Fig. 7. Comparison between the pulse height spectra for captured and scattered neutrons with the Karlsruhe energy resolution (left) and the expected resolution if only the fast component of the  $\text{BaF}_2$  scintillators were used (right). The neutron energy range was 10 keV to 100 keV. Response to scattered neutrons is indicated by the shaded spectrum. Note the importance of resolution in  $\gamma$ -ray energy.

### 5.3.3 Effect of using only the fast component of $\text{BaF}_2$ scintillation

In order to avoid pile-up effects at the higher neutron fluxes at spallation sources, it might be necessary to integrate only the fast component of the scintillator light, which contributes about 15% to the total light output. Correspondingly one would expect a reduction in energy resolution by a factor of  $\sqrt{7}$ . The effect of such a reduced energy resolution with respect to the background from capture in barium is shown in Fig. 7. For some samples, especially those with Q- values for neutron capture similar to those for barium isotopes, the degradation in resolution makes more difficult the separation of signal from this background of scattered neutrons captured in the scintillator.

### 5.3.4 Effects of sample backings

Possible backing materials for target preparation were investigated with respect to their background contributions due to neutron capture and scattering. Disk samples of 1 cm diameter were positioned in the center of the detector, and the thickness of the backing was assumed to equal the thickness of the gold sample. The results obtained for carbon and beryllium backings are summarized in Table 3, which compares the background due to scattering in the backing and the number of true capture events in the gold sample for different neutron energy intervals. The scattering contribution from the gold layer is listed separately for easier comparison.

The simulations show, not surprisingly, that the background is dominated by neutron scattering from the backing unless the sample thickness is consider-

Table 3

Background contributions from sample backings for a gold layer with the same thickness and diameter as the backing.

Backing	Backing-related events (scatter followed by capture in the scintillators)/true captures in a gold sample			
	0.1 to 1 keV	1 to 10 keV	10 to 100 keV	0.1 to 1 MeV
Carbon	0.33±0.02	0.50±0.04	1.13±0.13	1.21±0.36
Beryllium	0.51±0.02	0.80±0.05	1.77±0.18	1.43±0.40
Gold	0.52±0.02	1.09±0.04	1.34±0.10	3.19±0.60

ably larger than that of the backing. For example a 25  $\mu\text{m}$  beryllium substrate with a 0.5  $\mu\text{m}$  gold target (1 mg/cm<sup>2</sup>) would have a ratio of 90 scattered neutron events to 1 capture event in the 10 to 100 keV neutron energy region. Therefore sample diameters smaller than 1 cm are preferable. Titanium may be preferable as a backing material because of its high tensile strength and low neutron-capture cross section. Titanium was not evaluated in these simulations because the scattering cross sections were not in the GCALOR database.

### 5.3.5 Effect of beam pipe

The neutron beam from the spallation source will be in vacuum. Unlike the situation at Karlsruhe where the source is relatively close to the sample, the vacuum is necessary to eliminate neutron scattering from 20 to 200 meters of air, which would seriously degrade the beam quality. Furthermore, near the sample each cubic centimeter of air has approximately the same mass as the sample and therefore would contribute significantly to the effects of scattered neutrons. Gamma rays from capture on the sample as well as neutrons scattered from the sample will interact with the beam pipe. Selection of material for the beam pipe is critical. For aluminum, which has a small neutron capture cross section as well as a fairly low atomic number, most of the gamma rays will pass. Choosing a beam pipe with an outer diameter of 3 cm, some degradation in the total energy signal is observed when the pipe has a 3 mm wall thickness (see Fig. 15 in Ref. [27]).

### 5.3.6 Neutron absorbers

In order to reduce the background due to scattered neutrons, the possibility of absorbing scattered neutrons by suitable materials was investigated. For comparison with the unshielded configuration, three simulations are presented. First 0.8 mm thick layers of <sup>10</sup>B were inserted between the various BaF<sub>2</sub> crystals. Secondly, an inner 8 cm thick moderating neutron absorber of <sup>6</sup>LiH was placed just inside the inner radius of the BaF<sub>2</sub>-array. Finally a combination



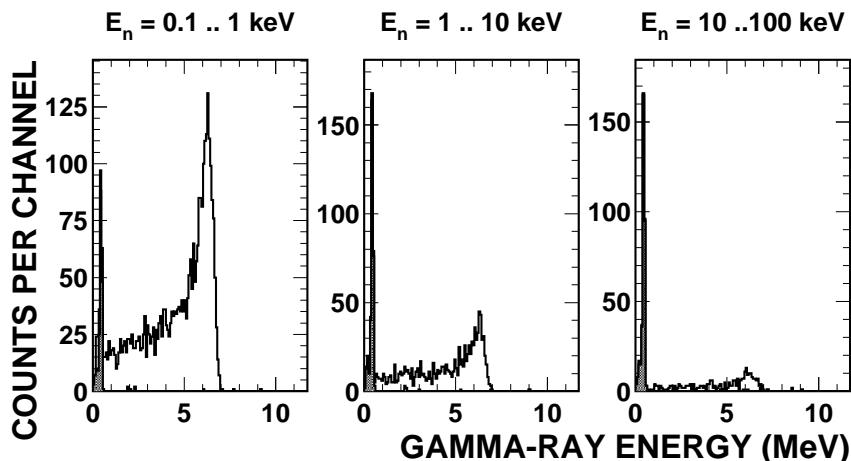


Fig. 8. The  $\gamma$ -ray spectra obtained with a spherical  ${}^6\text{LiH}$  absorber surrounding the sample and with thin  ${}^{10}\text{B}$  layers between the modules. The background from scattered neutrons (shaded regions) is almost eliminated. The line at low energies stems from the 478 keV transition following the  ${}^{10}\text{B}(n,\alpha)$  reaction.

of both approaches was simulated (see Fig. 8). In total, a background reduction by a factor 100 could be achieved in the astrophysically relevant region between 10 and 100 keV. The combination of the two absorbers was more effective than one might expect based solely on the simulations of the single absorbers.

It is apparent that including a  ${}^6\text{LiH}$  absorber may cause some degradation of the capture  $\gamma$ -ray spectrum. This effect is illustrated in Fig. 9 for different moderator/absorber thickness. A thick lithium hydride shell degrades the energy resolution of the detector and increases the low energy tail. Obviously the effect on the  $\gamma$ -rays is relatively small, however, since LiH consists of low- $Z$  elements.

The use of neutron absorbers as described above reduces the ratio of scattered neutron events to capture events in the 10 to 100 keV neutron energy region from 90 to 0.9 for a 1 mg gold target on a  $25\ \mu\text{m}$  beryllium substrate. This is sufficient to allow the further subtraction of scattered neutron events based on the energy spectrum. Greater improvement may be possible by using thinner target substrates such as titanium foils.

### 5.3.7 Detector granularity

The high granularity of a 162-element array introduces the possibility of analyzing the pattern of detectors that are hit in order to help discriminate between  $\gamma$ -ray and scattered-neutron induced events. This is not an easy problem, since gammas above 0.5 MeV interact primarily by Compton scatter and,

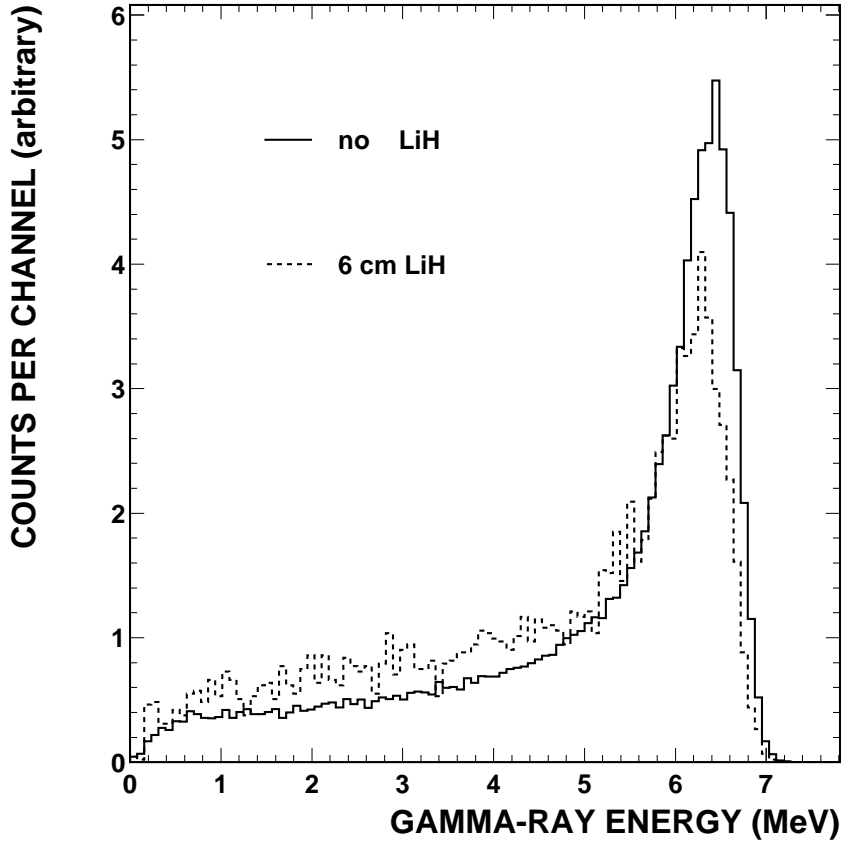


Fig. 9. Influence of a 6 cm thick  ${}^6\text{LiH}$  moderator/absorber layer on the shape of the  ${}^{197}\text{Au}(n, \gamma)$  spectrum.

at higher energies, by pair production, producing electron-gamma showers in the array. Thus, even single gammas can cause several crystals to fire. This is illustrated in Fig. 10, which shows the calculated multiplicity, or number of crystals that fire, for  $\gamma$ -rays of 2 and 6 MeV emitted at random angles from the center target position in the  $\text{BaF}_2$  ball. Gamma rays of other energies were also investigated in the range from 1 to 9 MeV. For almost all energies, multiplicity 2 is the most frequent. The average multiplicity ( $M$ ) was found to be a linear function of the  $\gamma$ -energy ( $E_\gamma$ ) in MeV,  $M = 0.154 \cdot E_\gamma + 1.44$ .

Sample hit patterns for multiplicities greater than two from monoenergetic 6 MeV gammas are shown in Fig. 11. The figure illustrates that the hit crystals do not have to be adjacent.

In an actual capture event, whether in the target or induced by a scattered neutron in a crystal, several gamma rays can be emitted resulting in a multiplicity distribution with the most probable multiplicity greater than 2. The simulations showed that there was no usable difference in the multiplicity dis-

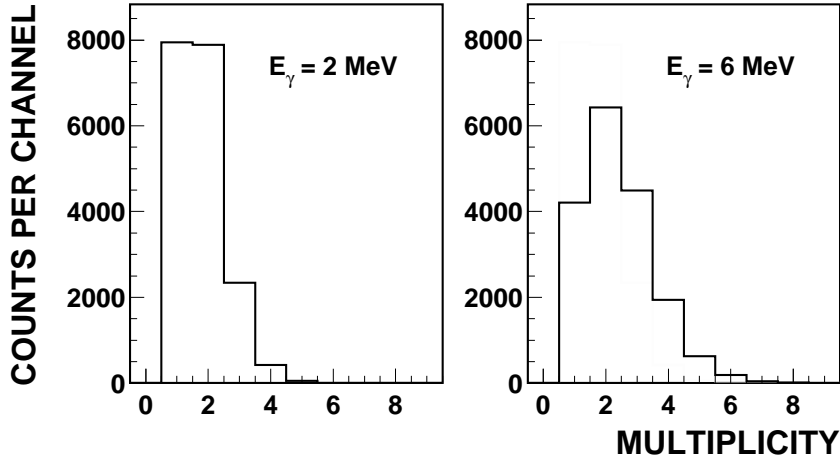


Fig. 10. Multiplicity distribution of detectors hit for monoenergetic  $\gamma$ -rays observed with the 162 module array.

tribution between capture and scatter events. However, captures that occur in a specific crystal, due to scattered neutrons, will produce several gammas which will most likely fire adjacent crystals. Multiple gammas produced by capture events in the target will most likely hit crystals in different regions of the array. Thus scatter events are expected to produce a single large cluster of hits, while capture events will produce multiple smaller clusters.

Clustering was analyzed in the simulation by tallying the number of hit clusters that occur for each event, the number of crystals that fire in the largest cluster, and the total energy deposited in the array divided by the number of clusters. A cluster was defined as a set of neighboring crystals that are all hit, and two crystals are defined as neighbors when the angle between two rays drawn from the center of the array to the center of each crystal is less than 20 degrees. As expected, the simulation showed that events due to scattered neutrons have fewer clusters, but more crystals are hit in the largest cluster. Fifty percent of events caused by scattered neutrons formed only one cluster.

Fig. 12 shows the distribution of the energy per cluster. The average energy extends higher in events caused by scattered neutrons. This is obvious since the total energy released as gammas is roughly the same for all reasonably heavy nuclei, but it can be all deposited in one cluster in a scatter event, while it is distributed over several clusters in a capture event. The best separation between events due to capture in the target and events due to scattered neutrons can be made by requiring that more than one cluster be formed, and that the average energy per cluster be less than 3.8 MeV. With these cuts, the ratio of scatter to capture events can be reduced by a factor of 3.

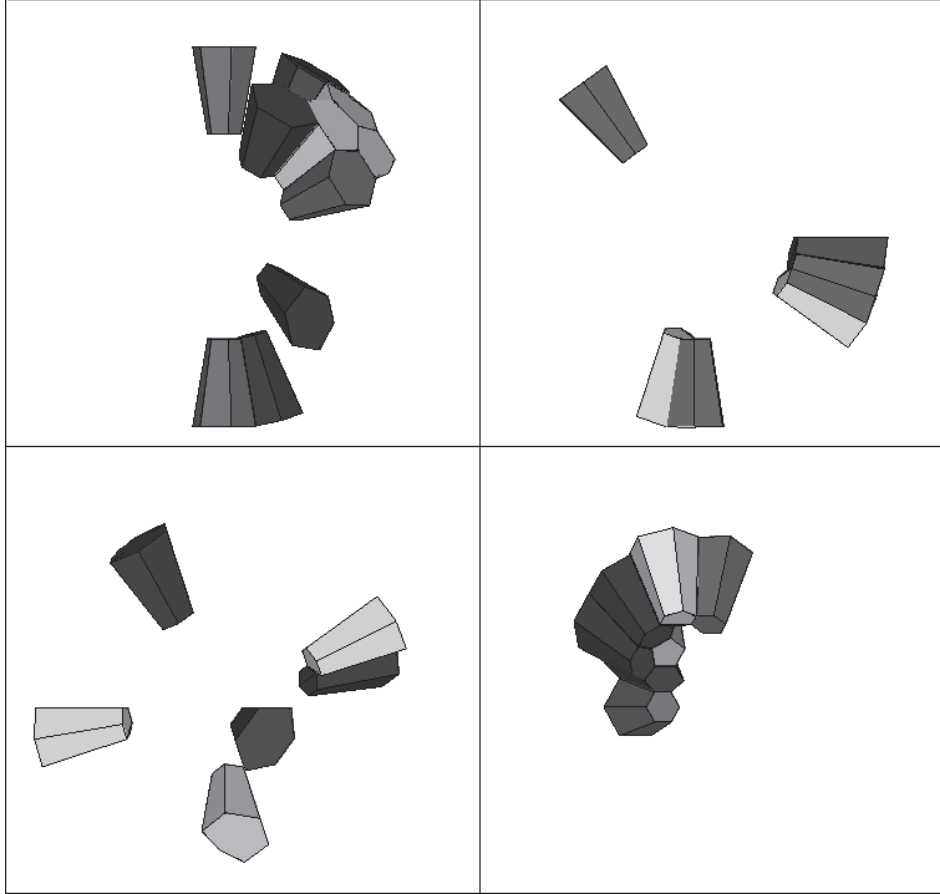


Fig. 11. Sample hit patterns for monoenergetic  $\gamma$ -rays of 6 MeV in the 162 module array. Shown are those modules which receive an energy deposit in excess of 50 keV. Obviously, hit patterns with higher multiplicities are not restricted to adjacent crystals.

It should be noted that the simulations were made with Au as a target. These results would be different if the  $\gamma$ -spectrum of the actual target were significantly different than that of Au. These results also relied on the energy resolution obtained by using both the fast and slow components of the BaF<sub>2</sub> crystal. If only the fast component were used, energy cuts may not be possible due to the poorer energy resolution (see below).

### 5.3.8 Other detector materials

Various scintillator materials can be used for  $\gamma$ -ray spectroscopy. In this section different scintillator materials are investigated with respect to their neutron sensitivity. Other properties, e.g. decay time of the scintillator light are not considered.

The setup used for the calculation was an array with 162 elements with an inner radius of 10 cm. The thickness of the crystals was chosen according to

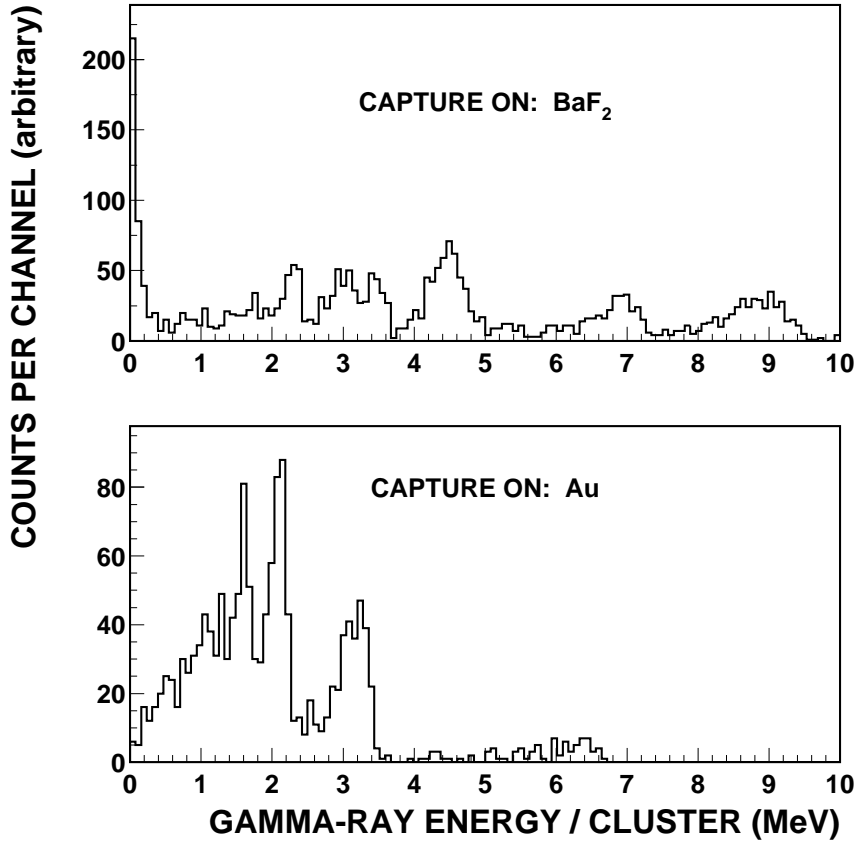


Fig. 12. Gamma-ray energy per cluster for neutron scatter events resulting in capture in the BaF<sub>2</sub> array (top) and for capture events in a gold sample (bottom). This difference provides a possible means of discriminating between capture and scatter events.

the attenuation length of the scintillator. An aluminum beam pipe of 3 mm thickness was also included. We assumed that the sample is 1 mm thick gold, located at the center of the array. This sample was irradiated with neutrons in the energy range from 0.1 eV up to 20 MeV. The energy spectrum of the neutrons was of the form  $1/E_n$  (see section 6.1) and the flight path was 20 m long. TOF spectra for events from neutron capture in the sample and for events from neutrons which were scattered on the sample and captured in the scintillator material were recorded separately. Various TOF cuts corresponding to neutron energy decades between 0.1 eV and 1 MeV were applied and the ratio between events caused by scattered and captured neutrons was calculated. The neutron scattering-to-capture ratio for these different bins varies from about 1:1 to more than 50:1. The response of the following scintillator materials was investigated by choosing the detector thickness such that the efficiency for capture events in the gold sample were equal in all cases.

- A  $\text{BaF}_2$ -array with a crystal thickness of 15 cm using the natural composition of barium.
- The same  $\text{BaF}_2$ -array but with the (hypothetical) assumption that only  $^{138}\text{Ba}$  was contained in the scintillator.
- A corresponding array of bismuth germanate (BGO) with a reduced thickness of 10 cm according to the higher  $\gamma$ -absorption. Since there are no photon data for neutron capture on germanium in the GCALOR data base, 2  $\gamma$ -rays with 25 % and 75 % of the full energy were assumed to be emitted in each capture event.
- $\text{CeF}_3$  represents an alternative solution requiring an intermediate crystal thickness of 13 cm.
- Finally a  $\text{C}_6\text{F}_6$  liquid scintillator tank with 120 cm diameter was considered for comparison. However, the resolution in  $\gamma$ -ray energy was so low that this possibility was not pursued any further.

In all these simulations, cladding of the scintillators and mechanical support structures were neglected.

The resulting neutron sensitivities are compared in Table 2. Since the  $\text{C}_6\text{F}_6$  solution is excluded because the limited light collection from large volumes deteriorates the resolution in  $\gamma$ -ray energy, one finds that  $\text{BaF}_2$  and BGO are about comparable, but that  $\text{CeF}_3$  is almost 10 times better at low neutron energies. However, this is the energy range where the scattering corrections are relatively small (see Fig. 6). In the important region above 10 keV this advantage is no longer very significant, in particular if one considers the effect of good neutron absorbers (Figs. 8 and 9) and the possibility of background separation using energy cuts (50% of the scattering events in  $\text{BaF}_2$  appear at energies above 7.5 MeV). Hence, the better energy resolution makes  $\text{BaF}_2$  still the scintillator of choice for a  $4\pi$  calorimeter.

#### 5.4 *Sample radioactivity*

Background caused by the decay of a radioactive sample may present a particular challenge. Usually, a decay deposits not more than about 1 MeV energy in the crystals whereas capture events deposit between 5 and 7 MeV. Therefore the problem is not deciding between single background and capture events but rather is related to the high radioactive count rate of a 1 mg sample with a lifetime between a few days and several years, resulting in massive pile up effects and dead time losses.

A listing of many isotopes of astrophysical interest is given in Table 4. For a sample mass of 1 mg the average number of counts in the detector system for an integration time of 150 ns (more than enough for the fast component)

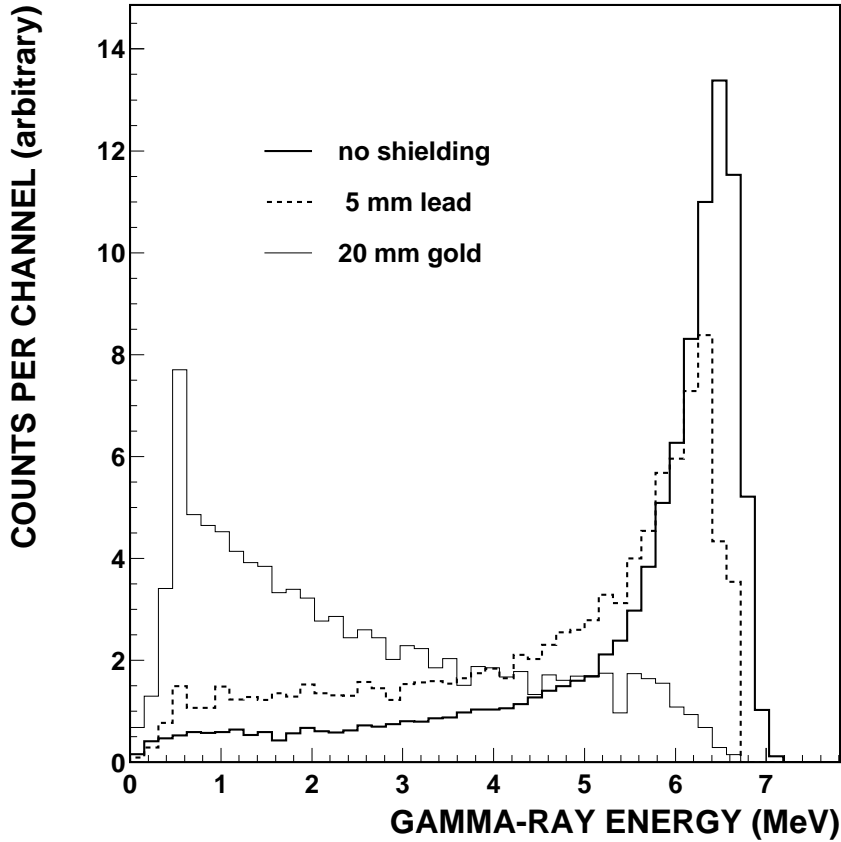


Fig. 13. Influence of various  $\gamma$ -shieldings on the  $^{197}\text{Au}(n, \gamma)$  spectrum.

and  $2 \mu\text{sec}$  (slow component) is given in columns 2 and 3, where we assume no shielding against radiation from the sample. In this case the probability of an accidental coincidence with true capture events would be unity for almost all of these isotopes. A lead shielding of 5 mm thickness would be sufficient to solve this background problem (columns 4 and 5) except for a few cases. The corresponding probabilities were calculated according to Poisson for the standard setup of 160 crystals assuming a spherical lead shielding of 5 mm thickness so that  $\gamma$ -rays from the sample in the center have to pass at least 5 mm lead. For a few isotopes a 5 mm thick lead shielding is not yet sufficient. Some of these, e.g.  $^{85}\text{Kr}$ ,  $^{170}\text{Tm}$ , and  $^{210}\text{Bi}$ , could still be measured if the lead shield is replaced by a 20 mm thick gold sphere [27]. Although it might not be practical because of its large  $(n, \gamma)$  cross section, gold was chosen for illustration due to its high atomic number and, compared with lead, its high density.

Shields of 5 mm lead and especially of 20 mm gold influence significantly the  $\gamma$ -ray resolution of the detector as shown for the detector response to  $^{197}\text{Au}(n, \gamma)$  cascades, in Fig. 13.

Table 4

Simulated background from some radioactive isotopes of astrophysical interest (sample mass 1 mg, see text). Isotopes marked by an asterisk are decay products of the isotope listed before with lifetimes shorter than the lifetime of the parent nucleus. Due to decay equilibrium the decay rates of daughter and parent isotope are equal.

Backing	No shielding		5 mm Pb		Radiation
	150 ns	2 $\mu$ s	150 ns	$P_{coinc}$	
$^{79}\text{Se}$	0.38	5.2	0	0	$\beta^-$ : 150
$^{85}\text{Kr}$	8.7	115	4.6	1	$\gamma$ : 514; $\beta^-$ : 700
$^{90}\text{Sr}$	770	1 $10^4$	0	0	$\beta^-$ : 550
$^{90}\text{Y}^*$	770	1 $10^4$	6.2	1	$\gamma$ : 1760; $\beta^-$ : 2.3 MeV
$^{94}\text{Nb}$	1.1	14	1.0	0.6	$\gamma$ : 871+703; $\beta^-$ : 470
$^{106}\text{Ru}$	1.8 $10^4$	2.4 $10^5$	0	0	$\beta^-$ : 40
$^{106}\text{Rh}^*$	1.8 $10^4$	2.4 $10^5$	3 $10^3$	1.0	$\gamma$ : 512; $\beta^-$ : 3.6 MeV
$^{135}\text{Cs}$	7 $10^{-3}$	0.1	0	0	$\beta^-$ : 200
$^{147}\text{Pm}$	13	180	0	0	$\gamma$ : 121; $\beta^-$ : 220
$^{151}\text{Sm}$	141	2 $10^3$	0	0	$\gamma$ : 20; $\beta^-$ : 80
$^{155}\text{Eu}$	1400	1.9 $10^4$	1.4 $10^{-3}$	1.4 $10^{-3}$	$\gamma$ : 87+105; $\beta^-$ : 250
$^{153}\text{Gd}$	2 $10^4$	2.6 $10^6$	1.5 $10^4$	1	$\gamma$ : 97+103; $\beta^+$ : 500
$^{163}\text{Ho}$	2.6	35	2.0	0.87	$\beta^+$ : 3
$^{169}\text{Er}$	4.5 $10^5$	6.0 $10^6$	0	0	$\gamma$ : 110; $\beta^-$ : 350
$^{170}\text{Tm}$	6.9 $10^3$	8.0 $10^4$	0	0	$\gamma$ : 84; $\beta^-$ : 1000
$^{171}\text{Tm}$	3.3 $10^4$	4.4 $10^5$	0.7	0.5	$\gamma$ : 67; $\beta^-$ : 100
$^{175}\text{Yb}$	9.4 $10^4$	1.2 $10^6$	2.4 $10^4$	1	$\gamma$ : 396; $\beta^-$ : 450
$^{182}\text{Hf}$	1.2 $10^{-3}$	1.6 $10^{-2}$	0	0	$\gamma$ : 270; $\beta^-$ : 160
$^{182}\text{Ta}^*$	1.2 $10^{-3}$	1.6 $10^{-2}$	1.2 $10^{-3}$	1.2 $10^{-3}$	$\gamma$ : 1.1+1.2 MeV; $\beta^-$ : 1.7 MeV
$^{185}\text{W}$	5.2 $10^4$	7.0 $10^5$	1.0 $10^{-5}$	1.0 $10^{-5}$	$\gamma$ : 125; $\beta^-$ : 430
$^{193}\text{Pt}$	0	0	0	0	no $\gamma$
$^{204}\text{Tl}$	66	880	0	0	$\beta^-$ : 800
$^{210m}\text{Bi}$	3.1 $10^{-3}$	4.2 $10^{-2}$	0	0	$\gamma$ : 266; $\alpha$ : 4.9 MeV



In spite of this degradation in energy resolution, the total efficiency for capture events is much less affected. In the ideal case considered, it drops from 100 % (without shielding) to 98.5 % for a 5 mm lead absorber. However, the massive gold shielding would result in a reduction to 54 % and would imply that the full energy peak disappears completely. But even in this extreme example the spectrum exhibits still enough events at high sum energies to allow for background discrimination.

### 5.5 Neutron beam profile

Collimation of the neutron beam for high energy neutrons (up to several hundred MeV) is much more difficult than collimation of lower energy neutrons. To investigate the problem of a beam halo produced by collimating the beam upstream of the sample, we assumed a beam core diameter of 30 mm (umbra), a penumbra of 80 mm diameter and an umbra/penumbra ratio of  $2 \times 10^5$ . The umbra was assumed to cover a gold sample 30 mm in diameter with a thickness of  $100 \mu\text{g}/\text{cm}^2$  for a total mass of 0.7 mg. The penumbra, after passing the sample position, was incident on the  $\text{BaF}_2$ . Even with this very small beam halo, the halo background was comparable to the neutron capture signal on the gold. Good collimation of the spallation neutron beam is therefore of great importance.

## 6 Summary

We have considered a  $4\pi$  array of  $\text{BaF}_2$  scintillators as a detector for neutron cross section measurements at a spallation neutron source. Many design options have been included in the Monte Carlo GEANT simulations.

We find that this type of detector, which detects the total  $\gamma$ -ray energy following the capture event, has significant advantages over other detectors in that capture on the sample can be differentiated from other events simply by the Q-value of the reaction. The energy resolution of the array must be good to take advantage of this essential feature. Factors that would worsen the resolution, such as incomplete energy collection or using only a fraction of the light (such as just the fast component from  $\text{BaF}_2$  crystals) or interaction of the  $\gamma$ -rays with components (such as the beam pipe, neutron absorbers, and aluminum and teflon reflectors around the scintillators) are quantified. If further discrimination against background is required, the hit patterns on highly segmented detectors can be used.

Effects of neutrons scattered from the sample can be significant, especially for those samples that have large scattering-to-capture ratios. The effects are particularly pronounced above 100 keV, where for most nuclei, the capture cross sections become quite small. Although  $\text{BaF}_2$  has a relatively small capture cross section, other scintillators such as  $\text{CeF}_3$  and  $\text{C}_6\text{F}_6$  can have even smaller cross sections, and their appropriateness for a given experiment should be kept in mind. Segmentation of the  $\text{BaF}_2$  was found to be a useful approach to identifying capture events from the sample and for discriminating against capture of scattered neutrons in the scintillator.

This study has not extended to data acquisition, where advanced techniques such as digital signal processing might be helpful especially when the instantaneous rate is high.

The detector designed here has many attractive features not only for neutron capture experiments but also for the study of  $\gamma$ -ray production in neutron-induced fission and neutron inelastic scattering.

Acknowledgments - This work has benefited from the use of the Los Alamos Neutron Science Center at the Los Alamos National Laboratory. This facility is funded by the U.S. Department of Energy and operated by the University of California under Contract No. W-7405-ENG-36. Three of us (M.H., F.K., R.R.) are grateful for the support of Los Alamos National Laboratory during several visits.

## References

- [1] P.W. Lisowski, C.D. Bowman, G.J. Russell, and S.A. Wender, Nucl. Sci. Engineering **106**, 208 (1990).
- [2] S. Abramovich *et al.*, Report CERN/SPSC 99-8; SPSC/P 310, CERN, Geneva, Switzerland (1999).
- [3] J.L. Ullmann *et al.*, in *Proc. 15th International Conference on the Applications of Accelerators in Research and Industry*, ed. J.L. Dugan and I.L. Morgan, AIP Conf. Proc. 475 (AIP, New York, 1999) 251.
- [4] J.B. Wilhelmy *et al.*, in *Proc. Second International Conference on Fission and Neutron-rich Nuclei*, University of St. Andrews, Scotland, June 28 to July 2, 1999 (to be published); and Report LA-UR-99-3376, Los Alamos National Laboratory, Los Alamos, USA (1999).
- [5] K.H. Guber, R.R. Spencer, P.E. Koehler, and R.R. Winters, Nucl. Phys. **A621**, 254c (1997).
- [6] K. Wisshak *et al.*, Phys. Rev. C **57**, 391 (1998).
- [7] A. Michaudon and S.A. Wender, Report LA-UR-90-4355, Los Alamos National Laboratory, Los Alamos, USA (1990).
- [8] D. Habs, F.S. Stephens, and R.M. Diamond, Report LBL-8945, Lawrence Berkeley Laboratory, USA (1979).
- [9] P.E. Koehler, Nucl. Instr. Meth. in Phys. Res. **A292**, 541 (1990).
- [10] K. Wisshak and F. Käppeler, Nucl. Instr. Meth. **227**, 91 (1984).
- [11] K. Wisshak *et al.*, Report KfK-4652, Kernforschungszentrum Karlsruhe (1989).
- [12] K. Wisshak *et al.*, Nucl. Instr. Meth. A **292**, 595 (1990).
- [13] M.C. Moxon and E.R. Rae, Nucl. Instr. Meth. **24**, 445 (1963).
- [14] S. Jaag and F. Käppeler, Phys. Rev. C **53**, 2474 (1996).
- [15] R.L. Macklin and J.H. Gibbons, Phys. Rev. **159**, 1007 (1967).
- [16] P.E. Koehler *et al.*, Phys. Rev. C **54**, 1463 (1996).
- [17] H. Beer, F. Corvi, and P. Mutti, Ap. J. **474**, 843 (1997).
- [18] J. Apostolakis, Technical report, CERN, GEANT library (available from: [www.cern.ch](http://www.cern.ch)).
- [19] C. Zeitnitz and T.A. Gabriel, Nucl. Instr. Meth. **A349**, 106 (1994).
- [20] ENDF-LIBRARY, National Nuclear Data Center, On-Line Access: [BNLND2.DNE.BNL.GOV](http://BNLND2.DNE.BNL.GOV), File ENDF; Brookhaven National Laboratory.
- [21] M. Uhl and J. Kopecky, in *Nuclei in the Cosmos 1992*, edited by F. Käppeler and K. Wisshak (Institute of Physics Publishing, Bristol, 1993), p. 259.
- [22] K. Wisshak *et al.*, Phys. Rev. C **52**, 2762 (1995).
- [23] N. Weber, thesis, University of Karlsruhe (1993).
- [24] K. Wisshak, F. Voss, F. Käppeler, and G. Reffo, Phys. Rev. C **45**, 2470 (1992).
- [25] F. Käppeler, in *Nuclei in the Cosmos V*, edited by N. Prantzos and S. Harissopulos (Editions Frontières, Paris, 1998), pp. 174 – 180.

- [26] H. Condé, R. Haight, H. Klein, and P. Lisowski, in *Nuclear Data for Science and Technology*, edited by S. Qaim (Springer, Berlin, 1992), p. 386.
- [27] M. Heil *et al.*, Report LA-UR-99-4046, Los Alamos National Laboratory, Los Alamos, USA (1999).